

Bubble statistics and coarsening dynamics for quasi-two dimensional foams with increasing liquid content

A. E. Roth, C. D. Jones, and D. J. Durian

Department of Physics & Astronomy, University of Pennsylvania, Philadelphia, PA 19104-6396, USA

(Dated: July 3, 2012)

We report on experiments in which foams are created and allowed to coarsen in a custom cell that permits the liquid content of the foam to be chosen and held constant for an extended period of time. With increasing liquid content the average coarsening rate decreases, and we are able to achieve a factor of four reduction from the dry limit. We observe that all samples evolve into a statistically self-similar scaling state, where distribution shapes are independent of time and are, furthermore, not affected by liquid content. In addition to usual quantities such as side number and area distributions, neighbor correlations, and size-topology correlations, we also report on bubble shape statistics and the area-weighted side number distribution. The latter is important for the rate of change of average bubble area. At the individual bubble level, we observe that von Neumann's law is systematically violated for small bubbles in a way that depends on liquid content. This effect is explained by a simplistic 'border-blocking' model, where the von Neumann argument is modified by assuming that gas diffusion is totally blocked by Plateau borders whose size inflates with wetness.

PACS numbers: 82.70.Rr

Coarsening is an evolution process in foams where gas diffuses from high to low pressure bubbles, so that the latter grow and the former shrink [1]. This is driven by a reduction of total interfacial surface energy, and causes the texture of the foam to become coarser with larger bubbles over time. Coarsening is not limited to foams and is also observed in other situations such as domain growth in metals. All coarsening systems share features and can be treated similarly [2, 3]. Foams, as a system, can be studied to understand coarsening behavior more generally. For two dimensional systems, John von Neumann [4] showed that the coarsening rate of a bubble or domain depends only on its number of sides as

$$\frac{dA_i}{dt} = K_0(n_i - 6), \quad (1)$$

where A_i and n_i are respectively the area and number of sides of bubble i . The constant of proportionality, K_0 , is proportional to the film tension, the solubility and diffusivity of the gas in the liquid, and inversely proportional to the film thickness. This relationship holds for mathematically ideal foams, which obey Plateau's laws and have zero liquid content.

There have been numerous experiments on two dimensional foams to measure coarsening rates and other properties, such as area and side number distribution functions. These include direct measurements on quasi-two dimensional soap froths contained between parallel plates [5–10], soap froths with different boundary conditions [11–13], and also measurements on lipid monolayers [14, 15]. Simulations have also been performed [16–21]. This entire body of work shows good general agreement with the von Neumann's law.

While the von Neumann's law describes the rate of change of area of individual bubbles, it can also be combined with bubble distribution information to predict how the average bubble area, $\langle A \rangle = \sum_i A_i / N_{tot}$, changes

over time. Since $\sum_i A_i = A_{tot}$ is the total sample area, the average area increases only by a decrease in the total number of bubbles, N_{tot} . The rate of change of average area is thus determined by the rate at which small bubbles disappear. Following the argument from Ref. [3], we start with the identity

$$\frac{\langle A^2 \rangle}{\langle A \rangle^2} \langle A \rangle = \frac{1}{A_{tot}} \sum_{i=1}^{N_{tot}} A_i^2 \quad (2)$$

with respect to time. When allowed to evolve, foams may reach a state in which they are self-similar over time, other than an increase in the average area. In particular, statistical quantities such as the normalized area and number of sides distributions do not change over time. This is called a scaling state. For foam in a scaling state, the quantity $\langle A \rangle^2 / \langle A^2 \rangle$ is a constant. Using this fact and von Neumann's law, we differentiate Eq. (2) and get

$$\frac{d\langle A \rangle}{dt} = 2K_0 \frac{\langle A \rangle^2}{\langle A^2 \rangle} \sum_n F(n)(n - 6), \quad (3)$$

$$= 2K_0 \frac{\langle A \rangle^2}{\langle A^2 \rangle} [\langle n \rangle - 6]. \quad (4)$$

In these equations $\langle A \rangle$ is the average bubble area, $\langle A^2 \rangle = \sum_i A_i^2 / N_{tot}$ is the average squared-area, and K_0 is the materials constant from von Neumann's law. The other quantity to appear is

$$F(n) = \sum_{i \text{ s.t. } n_i=n} A_i / A_{tot}, \quad (5)$$

the area-weighted side number distribution, which equals the probability that a randomly chosen point in space is inside an n -sided bubble. Note that $F(n)$ is distinct from the more usual side number distribution, $p(n)$, which equals the probability that a randomly chosen bubble has

n sides. Eq. (4) shows precisely how the evolution of the *average* bubble area depends on the distribution of bubbles, which in general would depend on time and on the history of the sample. It is not enough to know just the value of K_0 in von Neumann's law; it is also necessary to know the values of $\langle A \rangle^2 / \langle A^2 \rangle$ and the area-weighted average number of sides $\langle \langle n \rangle \rangle = \sum_n n F(n)$. Interestingly, neighbor correlations and the spatial arrangement of the bubbles play no role. While $\langle \langle n \rangle \rangle$, and the distribution $F(n)$, are thus crucial ingredients for understanding the evolution of coarsening foams, we are unaware of previous experimental or theoretical investigation of these quantities, though much is known about $p(n)$.

Coarsening in three dimensional foams has also been extensively studied, and the long-sought generalization of von Neumann's law is now known [22]. In terms of experiment, a variety of techniques have been used to study coarsening, include multiple light scattering [23–25], magnetic resonance imaging [26], optical tomography [27], x-ray tomography [28, 29], and observation of surface bubbles [30–34]. However it is much easier to measure two dimensional foams, where individual bubbles are readily imaged. Thus the level of contact between bubble-scale observations and growth laws is much greater in two dimensions.

One aspect of coarsening that has not been fully elucidated is the effect of non-zero liquid fraction, ϵ . Experiments on this effect have primarily focused on coarsening rates of three dimensional foams. One study suggested a mechanism for the reduced coarsening rate of three dimensional wet foams as the reduced film area due to liquid in the Plateau borders covering regions of the films and measured under forced drainage that the average coarsening rate was reduced by a factor of $(1 - \sqrt{\epsilon}/0.36)$ [25]. Another study measured coarsening rates for a freely draining three dimensional foam and using this model of Plateau border blocking film area measured that the average coarsening rate was reduced by a factor of $(1 - \sqrt{\epsilon}/0.44)^2$ [31]. Other studies on coarsening in three dimensional wet foams have found empirically that the average coarsening rate is reduced by a factor of $1/\sqrt{\epsilon}$ [32, 34]. In two dimensions, there has been theoretical [35–38] and simulation [35, 39] work on the effects of liquid content on coarsening. And while this paper was in preparation, a new theoretical approach was published for two dimensional wet foams, based on an effective number of sides that depends on the fraction of the turning radius occupied by wet versus dry interfaces [40]. The main result is that the average bubble radius grows as a power of time that decreases from $1/2$ to $1/3$ as the foam goes between dry and wet limits. Despite all this theoretical activity, we are unaware of any experiments that systematically examine the bubble-level effects of liquid content on coarsening.

In this paper we use a custom cell to create two dimensional foams with simple control of the liquid content. We use digital photography to measure individual bubbles as a function of both time and liquid content. The

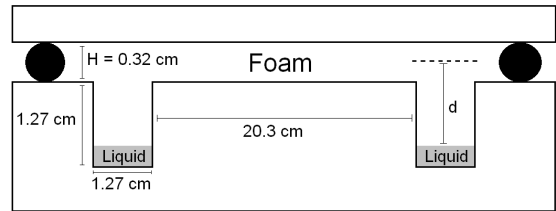


FIG. 1: Schematic vertical cross section of our circular constant pressure cell, not to scale. Imaging measurements are made in a central $11 \times 11 \text{ cm}^2$ region of interest. The foam wetness is controlled by the distance, d , of the liquid reservoir below the foam.

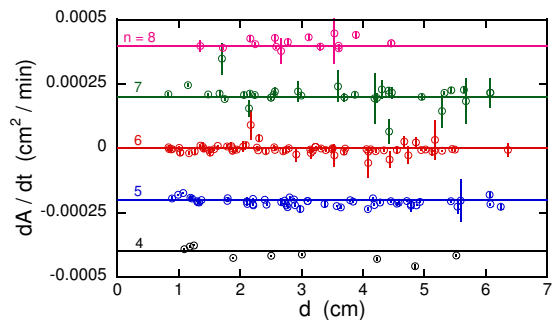


FIG. 2: (Color online) Rate of area change for individual bubbles in a vertical cell, versus the height of the bubble above the drained liquid. The number n of sides of each bubble is indicated by color, as labeled. The cell is the same cell from Fig. 1, but turned on end and filled 7.5 cm from the bottom of the O-ring. Symbol types distinguish bubbles with different number n of sides, as labeled. The lines on the plot are $dA/dt = K_0(n - 6)$ with $K_0 = 0.0002 \text{ cm}^2/\text{min}$.

results are analyzed in terms of probability distributions for bubble area, shape, and topology. These are found to be independent of liquid content, which is varied enough that the average coarsening rate changes by a factor of four. Thus we are able to average together the results for all runs to obtain very good statistics for distributions and for size-topology correlations in the scaling state. In terms of coarsening dynamics, the growth rates of individual bubbles are found to systematically deviate from von Neumann's law for small bubbles. We explain this behavior by developing a bubble-level border-blocking model of the effect of liquid content.

I. MATERIALS AND METHODS

The liquid foaming solution used here consists of 75% deionized water, 20% glycerin, and 5% Dawn Ultra Concentrated dish detergent. This creates foams that are stable and long lived; film ruptures were not observed. To characterize the solution in terms of the constant K_0 from Eq. (1), we created a vertical two dimensional cell. This cell consisted of a sealed circular chamber of di-

ameter 23 cm, with acrylic plates separated by a gap of 0.32 cm. This chamber is shown in horizontal cross section in Fig. 1. To create the foam, the chamber was completely filled with our solution. Pure nitrogen was then pumped into the chamber until only the desired amount of liquid remained. For this experiment the chamber was filled with solution to a height above the bottom of the O-ring of 7.5 cm. The chamber was then shaken vigorously until the chamber was filled with a uniform opaque foam consisting of bubbles much smaller than the spacing between the plates. The chamber was placed vertically and left to drain and coarsen until the foam consisted of a single layer of dry bubbles with almost all liquid at the bottom of the cell. This took about one day for this vertical cell. Note that the foam is not truly two-dimensional, because there are soap films that span the gap between the plates and because there are three-dimensional Plateau borders both running along the contact of individual films with the plates and also extending between the plates along the contact of three films.

For imaging, the sample cell was placed 20 cm in front of a Vista Point A light box and 2.5 m from a Nikon D80 camera with a Nikkor AF-S 300 mm 1:2.8 D lens. The camera was controlled by a computer to take pictures at two minute intervals. Since the soap films are perpendicular to the plates, we literally image the thick Plateau borders running along the plates. Using these photographs the bubble areas could be tracked over time and the coarsening rate of individual bubbles dA/dt could be measured. This data was plotted against the height of the bubble above the liquid reservoir and is shown in Fig. 2. We see that for a distance above the reservoir, d , greater than about 1 cm, the coarsening rate of each bubble is independent of height and varies only with the number n of sides. This means that the foam is in the dry limit, with constant film thicknesses, that the data can be fit to the form of Eq. (1). The solid lines in Fig. 2 give $K_0 = 0.0002 \text{ cm}^2/\text{s}$.

To control the liquid content of the foam, we built a circular constant pressure cell. A schematic vertical cross section can be seen in Fig. 1. This cell consisted of two 1.91 cm thick acrylic plates separated by a gap of 0.32 cm by an O-ring. The bottom plate had a trough of width and depth 1.27 cm and interior diameter 20.3 cm. This created a circular region of diameter 20.3 cm and height 0.32 cm that was the location for our foam. This same cell was, in fact, reoriented and used for the above dry-limit foam coarsening characterization.

The advantage of this chamber is that by adjusting the amount of liquid in the trough, it was possible to control the liquid content of the foam. In particular, the filling depth sets the height d of the foam above the top of the liquid in the trough. Decreasing d decreases the pressure drop in the foam and thus increases the liquid in the Plateau borders. The films of the foam are very thin and almost all liquid is stored in the Plateau borders, both the horizontal Plateau borders at the top and the bottom of the cell and the vertical Plateau borders at the

vertices where three films meet. The radius of curvature of the liquid in the Plateau borders is set by the capillary pressure, $P = \gamma/r$. For mechanical equilibrium, these capillary forces must exactly balance the gravitational pressure, $P = \rho g d$. This means that the relationship between this radius of curvature, r , and the height of the foam above the reservoir, d , is

$$r = \frac{\gamma}{\rho g d} \quad (6)$$

where γ is the surface tension, and ρ is the density of the liquid. As there is more liquid in the Plateau border, less area of the films is available for diffusion and thus the coarsening rate is slowed down. As proof of principle this effect can be seen in Fig. 3, where the area of selected bubbles of various n for three different foams of different liquid contents are plotted versus time. The rate of change of the area of an n sided bubble is related to the coarsening rate by von Neumann's law. We see here that as the foams become wetter, for decreasing d , the coarsening rate of the foam slows down. Thus our system design does indeed allow control of liquid content, in particular of the radius of curvature r of the Plateau borders, and through that the coarsening rate of the foam.

To create foam with N_2 gas bubbles, the chamber was prepared in the same method as the vertical cell, with the desired amount of liquid left remaining in the liquid reservoir trough. The foam was left to coarsen at least until there was a single layer of bubbles in the chamber. This initial coarsening took about two days. There was variation in the average bubble size at $t=0$, defined as the time at which the first picture was taken. This can be seen in Table I which shows the beginning and ending number of cells in a $11 \times 11 \text{ cm}^2$ square region of interest in the center of the cell. Only cells completely within the region of interest are considered.

d (cm)	N_{initial}	N_{final}
1.13	114	41
1.09	73	18
0.94	144	44
0.91	298	143
0.85	104	82
0.80	384	49
0.71	290	158
0.67	217	85
0.62	252	100

TABLE I: Initial and final numbers of bubbles in an $11 \times 11 \text{ cm}^2$ square region of interest in the center of the cell for different liquid contents. Only bubbles completely within the region of interest are considered.

After initial foam formation, the chamber was then placed horizontally 65 cm above a Vista Point A light box which provided constant illumination. A Nikon D80 camera with a Nikkor AF-S 300 mm 1:2.8 D lens was mounted 2.5 m above the chamber. The camera was

controlled remotely by a computer to take photographs at two minute intervals. The apparatus and sample cell would then be left undisturbed to collect photographs for durations between two days and two weeks.

To analyze a given image, the image was thresholded and skeletonized so that various descriptors of each bubble, such as area, number of sides, and center, could be measured. When a bubble's diameter becomes smaller than the distance between the plates, the bubble may 'pinch in' and a film will form horizontally in the middle of the bubble. This bubble is then not two dimensional. Bubbles like this were not considered in the analysis, and neither were their neighbors. Bubbles could be tracked between frames. To measure bubble dynamics, 30 frames in sequence were selected from a run of pictures. The images were then processed and the full set of descriptors were tracked for each bubble over time. This process was then repeated for other sets of frames taken at other times.

II. BUBBLE DISTRIBUTIONS

A. Bubble Side Distributions

The first relevant quantity to describe a bubble is the number of sides, since von Neumann's law states that the number of sides is the only relevant quantity in determining the time evolution of a bubble. Looking at this is also important because it can help establish whether our foam has reached a scaling state. If the foam is in a scaling state, the bubble side number distribution $p(n)$ should not change with time. We see in Fig. 4 data for a foam of fixed liquid content ($d = 0.91$ cm) at different times. We can see that there are no systematic changes in the side number distribution over time. Also in Fig. 4 we plot the area weighted bubble distribution function $F(n)$, and see that it also does not depend on time. This suggests that the foam is in a scaling state and that we can average together the probability distributions and area weighted probability distributions at different times to get an overall distribution for an entire liquid content. If we do this for all liquid contents we can see whether the side distribution depends on the liquid content and that data is plotted in Fig. 5. From this figure we observe no systematic dependence of the side number distribution or $F(n)$ on liquid content, which allows us to average together the probability distribution across all liquid contents. We can thus get an overall side distribution and an overall $F(n)$ for our system with good statistics and this is plotted in Fig. 6. There are a few things to note in this plot. Although 2 sided bubbles are possible, we never observed any. Likewise, we never observed any bubbles with more than 11 sides. This may be a function of our method of preparing the foam by shaking, which created an initial foam where all bubbles are small and similarly sized. The average number of sides that we observed was very close to 6, as we would

expect for topological reasons. Our side distribution is consistent with what others have observed [2, 3, 9, 17]. We also measured $F(n)$, the area-weighted bubble distribution function, which is also shown, averaged over all times and liquid contents, in Fig. 6. This is shifted to the right as compared to $p(n)$, because bubbles with many sides are on average larger than bubbles with fewer sides, as seen in Fig. 9. The area-weighted average side number is $\langle\langle n \rangle\rangle = 6.53 \pm 0.08$, which indeed is greater than six.

It is also possible to consider higher moments of side distributions. This includes the variance of the side number distribution, $\mu_2 = \sum (n - \langle n \rangle)^2 p(n)$. This is used as a measure of how disordered the foam is. Because our $p(n)$ does not depend on time or liquid content we can use our overall $p(n)$ distribution (Fig. 6) to calculate an overall μ_2 . The value we measure, $\mu_2 = 1.55 \pm 0.02$, is consistent with our foam being in a scaling state [7]. We can also define an area weighted variance, $\nu_2 = \sum (n - \langle\langle n \rangle\rangle)^2 F(n)$. We find $\nu_2 = 1.67 \pm 0.09$. Another quantity that people have looked at before is the quantity $m(n)$. This is the average number of sides among the neighbors of an n sided bubble. This is averaged over all n sided bubbles for a given snapshot. As with the ordinary number of sides distribution, $m(n)$ does not change over time and does not change with liquid content. This again allows us to average over all foams and get good statistics. The results can be seen in Fig. 7. There is a theoretical prediction for $m(n)$ called the Aboav-Weaire law which takes the form $m(n) = (6 - a) + (6a + \mu_2)/n$ where μ_2 we measure to be 1.56 ± 0.02 , and a is a fitting parameter. We find $a = 1.1 \pm 0.08$ which is within error of previous measurements [7]. Note that although the predicted curve fits generally well, the data appear to have slightly more curvature than the fit. Measurements of these distributions can be found in Table II.

B. Bubble Area Distributions

Another basic quantity of a bubble is its area. We can also look at how the distribution of bubble areas depends on time and liquid content. Fig. 8 shows the distribution of areas normalized by the average area at different times for a single liquid content ($d = 0.91$ cm). Although the average area increases with time, once this is divided out, the area distributions are constant in time. This suggests that the foam is in a scaling state. An exponential is shown for comparison, and the curves are consistent with previous experiments [2, 3, 9, 17]. Because the area distribution does not change over time, we can average together the distributions for all times for a single liquid content and compare the area distribution against the liquid content, which is also shown in Fig. 8. There is not any systematic variation of the area distribution with liquid content. Another relevant area related distribution to consider is the quantity $\langle A \rangle^2 / \langle A^2 \rangle$, which is relevant to the rate of change of the average bubble area, as seen in Eq. (4). Note that $\langle A \rangle^2 / \langle A^2 \rangle = 0.5$ for

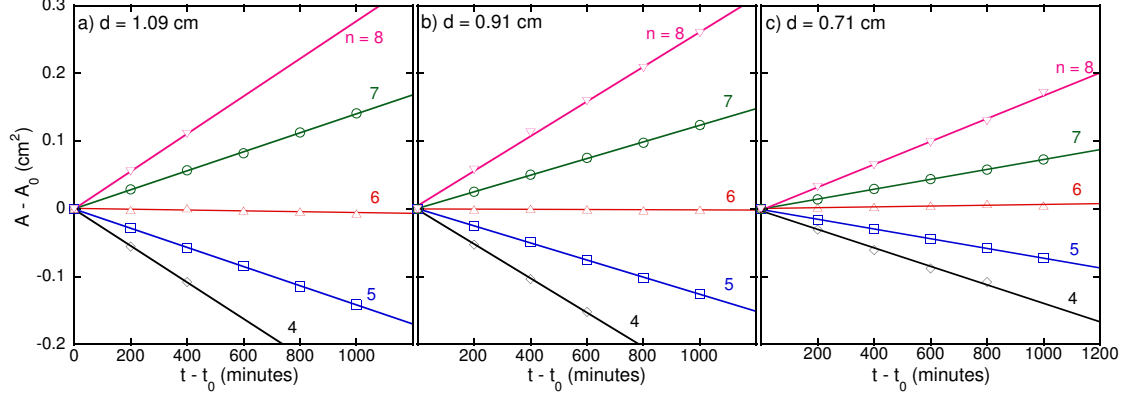


FIG. 3: (Color online) Area change versus time for select bubbles with different number of sides. Liquid contents increases from left to right plots as the distance, d , of the foam above the reservoir decreases. Note that the area change is linear and proportional to the number of sides. The lines are fits to the form $dA/dt = K(n - 6)$, with the same K used for all n . For part a) $K = 0.00014 \text{ cm}^2/\text{min}$, for part b) $K = 0.00012 \text{ cm}^2/\text{min}$, and for part c) $K = 0.00007 \text{ cm}^2/\text{min}$. Compare to Fig. 12, where dA/dt is plotted vs A for all bubbles in the same three samples.

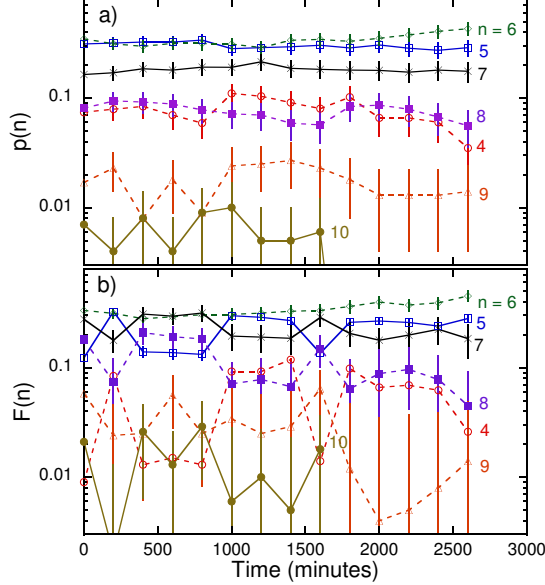


FIG. 4: (Color online) a) Side number distribution, and b) area-weighted side number distribution, versus time for a foam with $d = 0.91 \text{ cm}$.

the exponential area distribution $p(A) = \langle A \rangle^{-1} e^{-A/\langle A \rangle}$, which is shown for comparison in Fig. 8. Our measured value of $\langle A \rangle^2 / \langle A^2 \rangle = 0.58 \pm 0.09$ is consistent with the exponential distribution.

Because the number of side distribution and area distribution do not depend on time or liquid content, it is possible to average statistical quantities for all times and liquid contents and get good statistics. Results are collected in Table II and Table III. Note that our measurements and Eq. (4) give the average rate of coars-

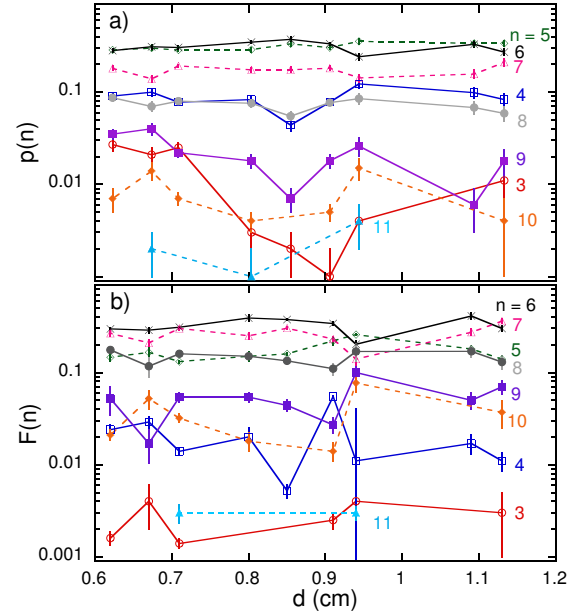


FIG. 5: (Color online) a) Side number distribution, and b) area-weighted side number distribution, plotted versus height of the foam above the liquid reservoir.

ening for a foam in the self-similar scaling state as $d\langle A \rangle/dt = (0.61 \pm 0.13)K_0$ where individual bubbles coarsen as $dA_i/dt = K_0(n_i - 6)$.

C. Bubble Shape Distributions

We can also consider other measures that depend on the area and number of sides in different ways. One pos-

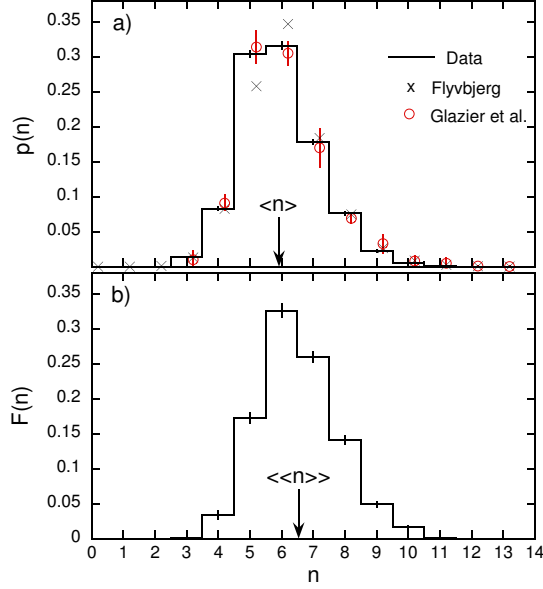


FIG. 6: (Color online) a) side number distribution, and b) area-weighted side distribution, averaged over all times for all liquid contents and plotted as a black histogram with error bars. The results are based on a total number of 11,663 bubbles. Bubbles with $n < 3$ or $n > 11$ were never observed; only eight 11 sided bubbles were observed. The prediction of Ref. [41] is shown by gray crosses. Previous experimental data from the table in Ref. [17] are shown by open red circles. The average, and area-weighted average, number of sides are indicated with an arrow.

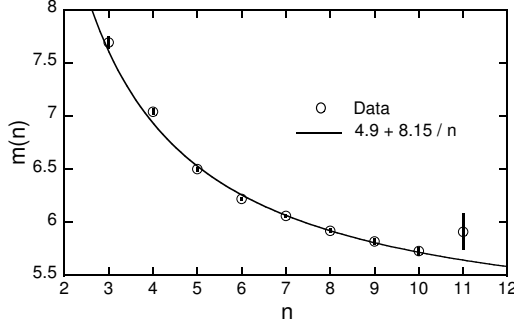


FIG. 7: Average number of sides of the neighbors of an n -sided bubble, plotted vs n . The points here are averaged over all times for all liquid contents. The black line is the Aboav-Weaire law, $m(n) = (6 - a) + (6a + \mu_2)/n$ where μ_2 is the variance, $\langle(n - \langle n \rangle)^2\rangle$, of the side distribution (for our system $\mu_2 = 1.56 \pm 0.02$) and a is the only fitting parameter, which we measure to be $a = 1.1 \pm 0.08$.

sible way to do this is to look at the average area of an n sided bubble. This is a relationship that has been of interest in the past [42]. The first empirical measurements were made by Lewis for epithelial cucumber cells, who

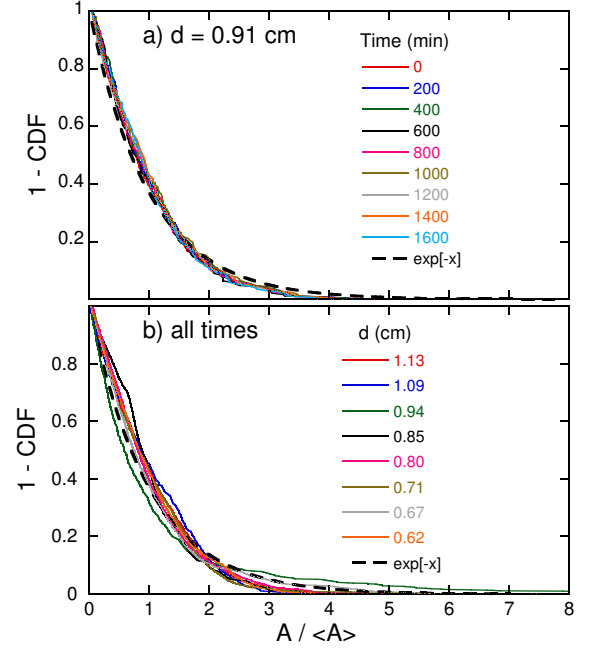


FIG. 8: (Color online) One minus the cumulative area distributions for a) foam with $d = 0.91$ cm at various times, and for b) foams of varying liquid contents. Specifically, $1 - CDF$ is the fraction of bubbles with normalized area greater than the $A/\langle A \rangle$. Dashed black curve is an exponential, shown for comparison. $\langle A \rangle^2 / \langle A^2 \rangle = 0.58 \pm 0.09$

Quantity	Definition	Value
$\langle n \rangle$	$\sum np(n)$	5.92 ± 0.01
μ_2	$\sum [n - \langle n \rangle]^2 p(n)$	1.56 ± 0.02
$\langle \langle n \rangle \rangle$	$\sum nF(n)$	6.53 ± 0.08
ν_2	$\sum [n - \langle \langle n \rangle \rangle]^2 F(n)$	1.67 ± 0.09
$\langle C \rangle$	$[\sum C]/N_{tot}$	1.0692 ± 0.0005
c_2	$\sum [C - \langle C \rangle]^2 / N_{tot}$	0.004 ± 0.001
$\langle A \rangle^2 / \langle A^2 \rangle$	$[\sum A_{i,n} / N_{tot}]^2 / [\sum A_{i,n}^2 / N_{tot}]$	0.58 ± 0.09

TABLE II: Definitions and measured values of relevant statistical quantities, averaged over all times and all liquid contents. In the definitions, n is the number of sides of a bubble, $p(n)$ is the fraction of bubbles with n sides, $F(n)$ is the fraction of area occupied by n sided bubbles, and $C = P/\sqrt{4\pi A}$ is a measure of the circularity of the bubble shape.

found a linear relationship of the form

$$\frac{\langle A_n \rangle}{\langle A \rangle} = n\lambda + (1 - 6\lambda) \quad \{Lewis\} \quad (7)$$

where λ is a parameter of the system [43, 44]. It is possible to show that if $\langle A_n \rangle / \langle A \rangle$ is linear in n , then it must have this form, but to prove linearity requires additional constraints [45]. Another related relationship of interest is how the average perimeter of an n sided bubble depends on n . The analogous relationship is called Desch's law or Feltham's law, and is the same as Lewis' law with

n	N	$p(n)$	$F(n)$	$m(n)$
3	195	0.013 ± 0.001	0.0009 ± 0.00006	7.69 ± 0.05
4	1217	0.083 ± 0.002	0.034 ± 0.006	7.04 ± 0.02
5	4462	0.304 ± 0.005	0.173 ± 0.007	6.5 ± 0.007
6	4634	0.316 ± 0.005	0.326 ± 0.009	6.22 ± 0.006
7	2611	0.178 ± 0.003	0.259 ± 0.007	6.06 ± 0.007
8	1120	0.076 ± 0.002	0.141 ± 0.006	5.92 ± 0.01
9	327	0.022 ± 0.001	0.049 ± 0.004	5.82 ± 0.02
10	89	0.006 ± 0.0006	0.016 ± 0.002	5.73 ± 0.03
11	8	0.0005 ± 0.0002	0.001 ± 0.0005	5.91 ± 0.16

TABLE III: Topological quantities averaged over all times and liquid contents, and their uncertainties: n is the number of sides; N is the total number of bubbles observed with n sides; $p(n)$ is the fraction of bubbles having n sides, and the uncertainty is the value divided by \sqrt{N} ; $F(n)$ is the fraction of area occupied by n sided bubbles, and the uncertainty is the standard deviation divided by the square root of the number of photographs; $m(n)$ is the average number of sides of the neighbors of an n sided bubble, and the uncertainty is the standard deviation divided by \sqrt{N} .

the area term replaced by the perimeter term. It has the form

$$\frac{\langle P_n \rangle}{\langle P \rangle} = n\nu + (1 - 6\nu) \quad \{Desch\} \quad (8)$$

where ν is a parameter of the system. It has been shown that if the average area of a cell is proportional to its perimeter, then the entropy is maximized when Desch's law is satisfied [46]. These relationships continue to be an area of theoretical and experimental interest [47–49].

We measured the normalized area for all bubbles, and the results, plotted as gray scale for all times and liquid contents, are shown in Fig. 9. The squares show the average normalized area for an n sided bubble, $\langle A_n \rangle / \langle A \rangle$. Note that the distribution of areas of n sided bubbles is not symmetric around the average, especially for bubbles with low n . Instead the areas are peaked near zero, and the average, shown as a square, is not near the center of the distribution. We see from the solid line that the form of Eq. (7) is a poor fit to the data. Additionally, allowing for a more general linear fit of the form $an + b$, where a and b are fitting parameters, shown as a dotted line, does not fit the data well either, nor does it match closely the fit to Lewis' law. This shows that Lewis' law is not appropriate for our data, and that the data is fit better by a quadratic form, in accordance with some simulations and experiments [47, 49].

We also measured the normalized perimeters for all bubbles, and the results, plotted as gray scale for all times and liquid contents, are shown in Fig. 10. The squares show the average normalized perimeter for an n sided bubble, $\langle P_n \rangle / \langle P \rangle$. Notice that the distributions in perimeter are much more symmetric than for the areas shown in Fig. 9. The fit to Eq. (8), shown as a solid line, fits the data well. Also, if the fit is allowed to take the more generic linear form $an + b$ where a and b are fitting parameters, the resulting fit, shown as a dotted line, matches very closely to the more constrained fit to Eq. (8). Desch's law describes our data more accurately than Lewis' law. The fitted value of ν from Eq. (8) is

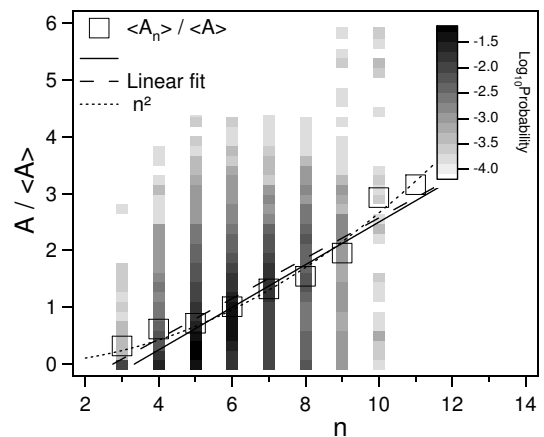


FIG. 9: Normalized area versus side number for all bubbles. The grayscale indicates the probability of finding a bubble with that side number and that area. Open squares are the average normalized area for a given n , $\langle A_n \rangle / \langle A \rangle$. The solid line is a fit to Lewis' law, Eq. (7), with fitted value $\lambda = 0.37 \pm 0.03$. The dashed line is a fit to the generic linear form $\langle A_n \rangle / \langle A \rangle = an + b$. The dotted curve is a fit to the proportionality $\langle A_n \rangle / \langle A \rangle = kn^2$ predicted in Ref. [49], with fitting value $k = 0.027$. Note that the distributions are quite skewed around the peak, as would be expected since the area distribution averaged over all n is nearly exponential.

0.15 ± 0.01 . This is somewhat smaller than previous experimental measurements of this quantity of 0.29 [47], and 0.19 [49], but the difference is not large compared to the range of these measurements.

It is also possible to look at a shape descriptor such as circularity. Circularity is defined as $P / \sqrt{4\pi A}$ where P is the perimeter and A is the area. This dimensionless number is equal to 1 for a circle and a large circularity would indicate a shape that is far from a circle. The distribution of circularities can be seen in Fig. 11. We see that the circularity does not depend on n , so it is possible to calculate an average circularity for all bubbles,

n	N	$\langle A_n \rangle / \langle A \rangle \pm \sigma \pm \sigma / \sqrt{N}$	$\langle P_n \rangle / \langle P \rangle$	$C(n)$
3	195	$0.32 \pm 0.59 \pm 0.04$	$0.46 \pm 0.42 \pm 0.03$	$1.065 \pm 0.02 \pm 0.001$
4	1217	$0.62 \pm 0.84 \pm 0.02$	$0.73 \pm 0.46 \pm 0.01$	$1.071 \pm 0.02 \pm 0.002$
5	4462	$0.72 \pm 0.70 \pm 0.01$	$0.843 \pm 0.38 \pm 0.006$	$1.070 \pm 0.03 \pm 0.001$
6	4634	$1.01 \pm 0.66 \pm 0.01$	$1.037 \pm 0.35 \pm 0.005$	$1.069 \pm 0.03 \pm 0.001$
7	2611	$1.32 \pm 0.77 \pm 0.02$	$1.183 \pm 0.40 \pm 0.008$	$1.070 \pm 0.02 \pm 0.001$
8	1120	$1.55 \pm 0.96 \pm 0.03$	$1.26 \pm 0.47 \pm 0.01$	$1.070 \pm 0.03 \pm 0.002$
9	327	$1.95 \pm 1.3 \pm 0.07$	$1.41 \pm 0.54 \pm 0.03$	$1.067 \pm 0.04 \pm 0.002$
10	89	$2.9 \pm 2.0 \pm 0.2$	$1.72 \pm 0.70 \pm 0.08$	$1.065 \pm 0.01 \pm 0.001$
11	8	$3.2 \pm 3.7 \pm 1.3$	$1.7 \pm 1.2 \pm 0.4$	$1.066 \pm 0.01 \pm 0.005$

TABLE IV: Size and shape quantities averaged over all times and liquid contents, with the standard deviation of the distribution and the uncertainty in the mean: n is the number of sides; N is the total number of bubbles observed with n sides; $\langle A_n \rangle / \langle A \rangle$ is the average normalized area of an n sided bubble; $\langle P_n \rangle / \langle P \rangle$ is the average normalized perimeter of an n sided bubble; and $C(n)$ is the average circularity of an n sided bubble.

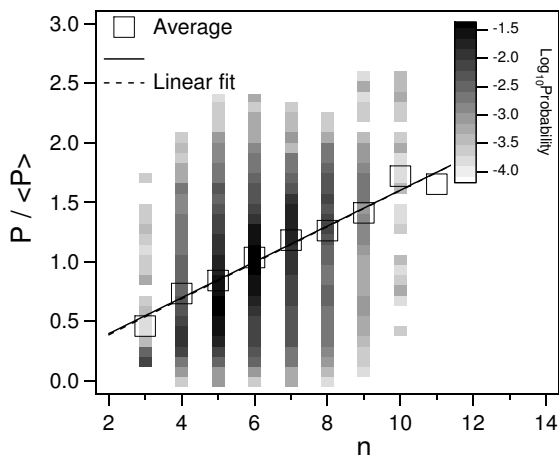


FIG. 10: Normalized perimeter versus side number for all bubbles. The grayscale indicates the probability of finding a bubble with that side number and that perimeter. Open squares are the average normalized perimeter for a given n , $\langle P_n \rangle / \langle P \rangle$. The solid line is a fit to Desch's law, Eq. (8), with fitted value $\nu = 0.15 \pm 0.01$. The dotted line is a fit to the generic linear form $\langle P_n \rangle / \langle P \rangle = an + b$. Note that for a given n , the distribution is much more symmetric around the peak than in Fig. 9.

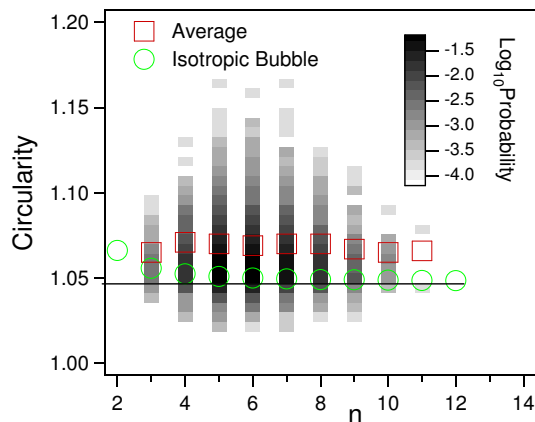


FIG. 11: (Color online) Circularity versus side number for all bubbles. Circularity is defined as $C = P / \sqrt{4\pi A}$, where P is perimeter and A is area. The grayscale indicates the probability of finding a bubble with that side number and that circularity. Red squares are the average circularity for a given n . Green circles show the circularity for an isotropic bubble with n sides. The line is the limit of the circularity of an isotropic n -sided bubble as n goes to infinity.

III. BUBBLE DYNAMICS

$\langle C \rangle = 1.0692 \pm 0.0005$, and a variance for the circularity, $c_2 = 0.004 \pm 0.001$, as shown in Table II. For comparison, the circularity of a perfectly isotropic bubble of n sides is shown on the plot. An isotropic bubble is a regular n sided polygon with the sides replaced with circular arcs of identical curvature necessary to satisfy Plateau's laws. Note that most bubbles have a circularity slightly larger than a perfectly isotropic bubble of the same number of sides, but there is a distribution around this. There is variation in bubble shape, but most bubbles are not too far from the isotropic bubble, which is a bubble with all sides the same length and all sides having the same curvature. This is related to the isotropic bubble approximation used in developing our model later in the paper.

All measurements discussed so far have been for individual static photographs and have not involved how individual bubbles change over time. It is also possible to track individual bubbles over time and observe how various quantities change. This was shown earlier, in Fig. 3, for select bubbles of various n for three liquid contents. In this plot it can be seen that the rate of change of an n -sided bubble's area is slower for wetter foams.

It is possible to measure the area at each time for each bubble in a sequence of images and fit these curves to a line for each bubble. The slope is dA/dt for that bubble. In this way it is possible to measure dA/dt for a large number of bubbles. We can then plot dA/dt against area for a given liquid content. Examples of this for

three different liquid contents are shown in Fig. 12. In these graphs each point is one bubble and the color indicates the number of sides. The horizontal lines are $dA_n/dt = K(n-6)$ for various n where K is the slope of the proportionality when the data on the plot is plotted as dA/dt against $n-6$. On these plots, K , the coarsening rate, is the spacing between these horizontal lines. The values of K are shown against liquid content in Fig. 13. The first thing to note is that the coarsening rate decreases as the liquid content increases. This makes sense as more liquid in the foam should prevent diffusion. Note also that there is a deviation from von Neumann's law for small bubbles. Von Neumann's law predicts that all bubbles with a given number of sides should coarsen at the same rate, so that means that in these graphs all points of a particular color should fall on the horizontal line of the same color. Instead, we see that small 4 and 5 sided bubbles fall above the appropriate line, which is to say they are shrinking more slowly than predicted. Very small bubbles with $n > 5$ are not observed because by the time the foam has become two dimensional, there are no very small bubbles with $n > 5$ and these bubbles do not shrink, so no examples ever become small enough to observe this effect. Note also that this deviation appears to be greater for higher liquid contents.

IV. MODEL

We wish to understand the effects of increasing liquid content, both in slowing of coarsening rate and in causing a deviation of small bubbles from von Neumann's law. The new model of Ref. [40] is for a truly two dimensional foam, with no Plateau borders along the top and bottom plates, and implies that $d\langle A \rangle/dt$ is not linear in time. Therefore we must construct our own model. To this end we invoke the 'border blocking' idea of Refs. [25, 31, 35]. Such models approximate that all liquid is stored in the Plateau borders and that the borders totally blocks gas diffusion, creating an effective film area smaller than the actual film area and slowing coarsening. While the prior models dealt only with average growth rates, we now consider the effect of border blocking on individual bubbles through a modification of von Neumann's law.

To begin, we take $dA/dt \propto \sum U_i \Delta P_i$, where U_i is the unblocked area of film i , and ΔP_i is the pressure across film i for any given bubble. For simplicity we also approximate that the liquid in the Plateau borders has a radius of curvature, r , everywhere the same, both on the top and bottom plates and in the vertical Plateau borders where three films meet. The expected relationship between this r and the measured value d based on capillarity is $r = \gamma/\rho g d$ (Eq. (6)) where γ is the surface tension and ρ is the density of the liquid. We also assume that the vertical Plateau borders are symmetric. This means that there is a blocked region of height r at the top and bottom of the plates and that the length of the film is reduced by $r/\sqrt{3}$ at each end. This means that for a film

of length L , height H , radius of curvature R , and Plateau borders of radius r , the unblocked area across which gas diffuses will be $U = (L - 2r/\sqrt{3})(H - 2r)$. The pressure across the film will be $\Delta P = \gamma/R$ where R is the radius of curvature of the film. We can now apply the same type of argument as used by von Neumann in Ref. [4] using our unblocked film area, U instead of the standard area of the film. Plateau's laws require films that are circular arcs and threefold vertices that meet at angles of $2\pi/3$. Therefore, the turning angle across a film is L/R , and the turning angle at a vertex is $\pi/3$. We know that the sum of the turning angles around an entire bubble must be equal to 2π , which with some rearrangement gives

$$\frac{dA}{dt} = K_0 \left(1 - \frac{2r}{H}\right) \left[(n-6) + \frac{6r}{\pi\sqrt{3}} \sum_i \kappa_i \right]. \quad (9)$$

In this equation $\kappa_i = 1/R_i$ is the curvature of side i and K_0 is the constant from von Neumann's law for a perfectly dry foam (see Eq. (1)). Note that the overall coarsening rate is reduced with liquid content by a factor $(1 - 2r/H)$ that is the same for all bubbles. However, there is also a term $\sum_i \kappa_i$ that depends on the shape of the bubble and that causes a deviation from the usual $(n-6)$ von Neumann behavior.

The von Neumann violating term $\sum_i \kappa_i$ in Eq. (9) does not have a general simple form. However, we can gain insight into the consequence of this extra term by treating bubbles as isotropic, similar to the approaches in Refs. [50–53] for approximating three dimensional foam coarsening. In particular, bubbles are assumed to be regular polygons, but with the edges replaced by circular arcs that have turning angles of $2\pi/3$ at the vertices in order to satisfy Plateau's laws. Then the sum of curvatures may be calculated to be

$$\sum_i \kappa_i = \frac{2n}{a} \sin\left(\frac{\pi}{n} - \frac{\pi}{6}\right) \quad (10)$$

where a is the side length of the regular straight sided n sided polygon that is used in the definition of the isotropic bubble. This vanishes for $n = 6$, and shows that deviation from the von Neumann law should be more pronounced for smaller bubbles. To express Eq. (10) in terms of bubble area, so that we may compare to data, we first note that the area of an isotropic bubble can be written

$$A = \frac{na^2}{4} \cot\left(\frac{\pi}{n}\right) + \frac{na^2}{8 \sin\left(\frac{\pi}{n} - \frac{\pi}{6}\right)} \left(\frac{2\pi}{n} - \frac{\pi}{3} - \sin\left(\frac{2\pi}{n} - \frac{\pi}{3}\right) \right) \quad (11)$$

where the first term is the area of the regular polygon, and the second term is the difference due to the arc regions. Solving Eq. (11) for a , plugging it into Eq. (10), and plugging that result into Eq. (9) gives the final result

$$\frac{dA}{dt} = K_0 \left(1 - \frac{2r}{H}\right) \left[(n-6) + f(n)rA^{-\frac{1}{2}} \right] \quad (12)$$

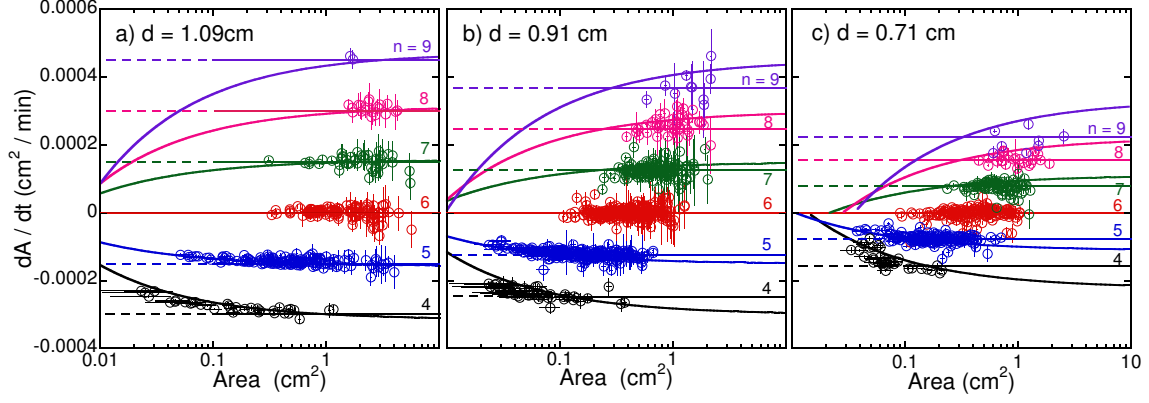


FIG. 12: (Color online) Rate of area change versus area, for all bubbles in three foam with a) $d = 1.09$ cm, b) $d = 0.91$ cm, and c) $d = 0.71$ cm. The liquid content increases from left to right as the distance of the foam above the liquid reservoir is reduced. Color corresponds to number of sides of a bubble, n . Von Neumann's law predicts that all bubbles with the same number of sides will coarsen at the same rate (see Eq. (1)). Note that there seems to be a deviation from this for very small bubbles. There are two fits included on these graphs. The first is the thin lines on the graph, which are fits to $dA/dt = K(n-6)$ where K is fit to the data for $A > 0.1 \text{ cm}^2$, with bubbles that deviate from von Neumann's law excluded. The values of K for different liquid contents are shown in Fig. 13. The second is the heavy lines, which are model predictions of the form $dA/dt = K_0(1 - 2r/H)[(n-6) + f(n)rA^{-1/2}]$ (see Eq. (12)), where $K_0 = 0.0002 \text{ cm}^2/\text{min}$ is a constant derived from the data in Fig. 2 and r is the only fitting parameter. Fig. 14 shows the fitted values of r against liquid content.

where

$$f(n) = \frac{12n}{\pi\sqrt{3}} \sin\left(\frac{\pi}{n} - \frac{\pi}{6}\right) \left[\frac{n}{4} \cot\left(\frac{\pi}{n}\right) + \frac{n}{8 \sin^2\left(\frac{\pi}{n} - \frac{\pi}{6}\right)} \left(\frac{2\pi}{n} - \frac{\pi}{3} - \sin\left(\frac{2\pi}{n} - \frac{\pi}{3}\right) \right) \right]^{\frac{1}{2}} \quad (13)$$

For comparing to data, this equation has only two parameters, K_0 and r . Because K_0 is the constant from von Neumann's law for a perfectly dry foam, we fix its value as measured in Fig. 2. Our model for dA/dt now only has a single fitting parameter, r . This parameter shows up in two places. First, it appears in the initial coefficient $K_0(1 - 2r/H)$ that sets the overall coarsening rate. Second, it appears in the extra term $f(n)rA^{-1/2}$ that sets the deviation from von Neumann's law.

We fit Eq. (12) to our data in two ways. The first is to plot dA/dt versus $n-6$ for each bubble for a given liquid content, and fit an overall coarsening rate, K . Small bubbles with area $< 0.1 \text{ cm}^2$ were not included because they deviate from von Neumann's law. We do this for each liquid content and the results for K are plotted in Fig. 13 vs the height d of the foam above the liquid reservoir. The expectation, $K = K_0(1 - 2r/H)$ with $r = \gamma/\rho g d$ and $\gamma = 25 \text{ dynes/cm}$, is also shown for comparison. The trend is correct, but not quantitatively so. Allowing for r to be different at the top and bottom plates due to their difference in height improves the agreement, which is shown as a dotted line on the graph.

It is also possible to directly fit dA/dt vs A data shown in Fig. 12 to the form of Eq. (12) by adjusting the value

of r . Only data for 4 and 5 sided bubbles was used to calculate a fit for r because only these bubbles included small bubbles that deviated from von Neumann's law. The model predictions are shown as the heavy lines in Fig. 12. We see that the model predictions fit the coarsening rate data quite well. We can now consider whether these fitted versions of r conform with our expectation based on the heights of the foam above the liquid reservoir. This data is shown in Fig. 14. The points are the fitted values of r and the solid line is our expectation using γ of 25 dynes/cm. The line does not fall directly on the points, but is qualitatively comparable. The dotted line is again a correction for variation in r due to the height of the cell, and improves the fit.

Our model is simplistic and makes incorrect assumptions, including isotropic bubbles, a constant r for the Plateau borders, that the Plateau borders totally block diffusion, and that the liquid in the vertical Plateau borders does not cause deviation in the angles from Plateau's laws. Despite these problems, the model qualitatively fits the data well and explains the deviation from von Neumann's law for small wet bubbles.

V. CONCLUSION

We measured quasi-two dimensional foam coarsening in a constant pressure cell. Image analysis allowed the processing of a large quantity of data and good statistics for the scaling state. Our data for the side number distribution, for the Aboav-Weaire law, and for the area distribution are all in good accord with prior work

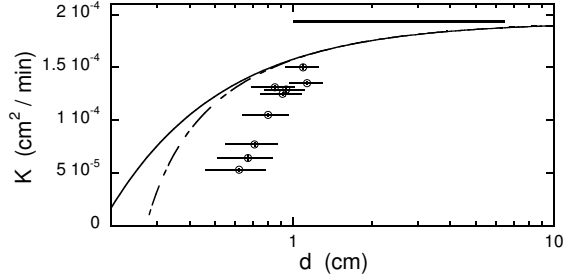


FIG. 13: Coarsening rate $K = (dA_n/dt)/(n-6)$ versus height above the liquid reservoir. These fits correspond to the thin lines in Fig. 12. The solid curve is the predicted relationship $K = K_0(1 - 2r/H)$, where K_0 is the observed coarsening rate for very dry bubbles ($1 \text{ cm} < d < 6 \text{ cm}$), shown as a horizontal line. This corresponds to the thin lines in Fig. 2. The dotted line is the expected K if we allow the top and bottom plates to have different r owing to the height of the cell.

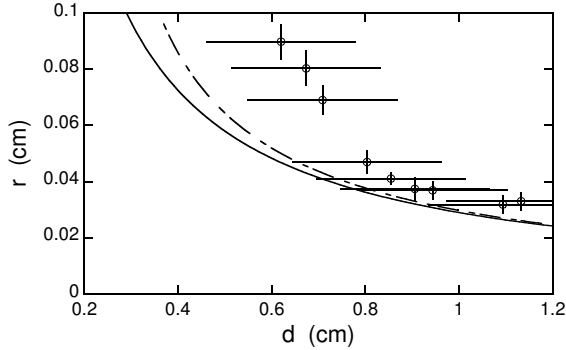


FIG. 14: Fitted value r versus height of the foam above the reservoir. These fits for r come from fitting the data as in Fig. 12 to the form of Eq.(12). These fits for r correspond to the heavy lines in Fig. 12. The solid curve is the expected relationship $r = \gamma/\rho g d$. The dotted curve is the expected average r if we allow the top and bottom plates to have a different r owing to the height of the cell.

but have improved statistics in comparison with prior experimental state-of-the-art. We also measured other important statistical quantities, like the fraction $F(n)$ of the sample area in n -sided bubbles, the area-weighted average side number, $\langle\langle n \rangle\rangle$, and the circularity of the bubble shapes, which to our knowledge have not been previously considered. For size-topology correlations, we find that Desch's law is a better description of our system than Lewis' law. For coarsening dynamics, we measured the rate of area change of individual bubbles and found general accordance with von Neumann's law, but with a systematic deviation for small bubbles. We also controlled the liquid content of the foam and were able to observe how this changed the coarsening rate. We developed a simple 'border blocking' model for the effect of liquid content that was able to qualitatively describe both this change in coarsening rate and the deviation from von Neumann's law for small bubbles. Altogether our work significantly enforces and complements existing data, and shows how wetness can play a surprisingly dramatic and bubble-specific role in coarsening. We hope this might help point the way for future studies of bubble-scale behavior in the coarsening of wet three-dimensional foams.

Acknowledgments

This work was supported by NASA Microgravity Fluid Physics Grant NNX07AP20G.

-
- [1] D. Weaire and S. Hutzler, *The Physics of Foams* (Oxford University Press, New York, NY, 1999).
 - [2] J. Glazier and D. Weaire, *J. Phys.: Condens. Matter* **4**, 1867 (1992).
 - [3] J. Stavans, *Rep. Prog. Phys.* **56**, 733 (1993).
 - [4] J. von Neumann, in *Metal Interfaces* (American Society for Metals, Cleveland, 1952), pp. 108–110.
 - [5] J. A. Glazier, S. P. Gross, and J. Stavans, *Phys. Rev. A* **36**, 306 (1987).
 - [6] J. A. Glazier and J. Stavans, *Phys. Rev. Lett.* **40**, 7398 (1989).
 - [7] J. Stavans and J. A. Glazier, *Phys. Rev. Lett.* **62**, 1318 (1989).
 - [8] J. Stavans, *Phys. Rev. A* **42**, 5049 (1990).
 - [9] J. Stavans, *Physica A* **194**, 307 (1993).
 - [10] M. de Icaza, A. Jiménez-Ceniceros, and V. M. Castaño, *J. Appl. Phys.* **76**, 7317 (1994).
 - [11] O. Krichevsky and J. Stavans, *Phys. Rev. B* **46**, 10579 (1992).
 - [12] M. E. Rosa and M. A. Fortes, *Philos. Mag. A* **79**, 1871 (1999).
 - [13] A. E. Rosa, L. Afonso, and M. A. Fortes, *Philos. Mag. A* **82**, 2953 (2002).
 - [14] K. J. Stein, S. A. Raueo, and B. G. Moore, *Phys. Rev. A* **41**, 6884 (1990).
 - [15] B. Berge, A. J. Simon, and A. Libchaber, *Phys. Rev. A* **41**, 6893 (1990).
 - [16] J. P. Kermode and D. Weaire, *Computer Phys. Comm.* **60**, 75 (1990).
 - [17] J. Glazier, M. Anderson, and G. Grest, *Philos. Mag. B* **62**, 615 (1990).
 - [18] T. Herdtle and H. Aref, *J. Fluid Mech.* **241**, 233 (1992).
 - [19] D. Segel, D. Mukamel, O. Krichevsky, and J. Stavans, *Phys. Rev. E* **47**, 812 (1993).

- [20] L. Neubert and M. Schreckenberg, *Physica A* **240**, 491 (1997).
- [21] A. D. Rutenberg and M. B. McCurdy, *Phys. Rev. E* **73**, 011403 (2006).
- [22] R. D. MacPherson and D. J. Srolovitz, *Nature* **446**, 1053 (2007).
- [23] D. J. Durian, D. A. Weitz, and D. J. Pine, *Science* **252**, 686 (1991).
- [24] D. J. Durian, D. A. Weitz, and D. J. Pine, *Phys. Rev. A* **44**, 7902 (1991).
- [25] S. Hutzler and D. Weaire, *Philos. Mag. Lett.* **80**, 419 (2000).
- [26] C. P. Gonatus, J. S. Leigh, A. G. Yodh, J. A. Glazier, and B. Prause, *Phys. Rev. Lett.* **75**, 573 (1995).
- [27] C. Monnereau and M. Vignes-Adler, *Phys. Rev. Lett.* **80**, 5228 (1998).
- [28] J. Lambert, I. Cantat, R. Delannay, A. Renault, F. Graner, J. A. Glazier, I. Veretennikov, and P. Cloetens, *Coll. and Surf. A* **263**, 295 (2005).
- [29] J. Lambert, R. Mokso, I. Cantat, P. Cloetens, J. A. Glazier, F. Graner, and R. Delannay, *Phys. Rev. Lett.* **104**, 248304 (2010).
- [30] B. S. Gardiner, B. Z. Dlugogorski, and G. J. Jameson, *Philos. Mag. A* **80**, 981 (2000).
- [31] S. Hilgenfeldt, S. A. Koehler, and H. A. Stone, *Phys. Rev. Lett.* **86**, 4704 (2001).
- [32] M. U. Vera and D. J. Durian, *Phys. Rev. Lett.* **88**, 088304 (2002).
- [33] A. M. Gañán-Calvo, J. M. Fernandez, A. Marquez Oliver, and M. Marquez, *Appl. Phys. Lett.* **84**, 4989 (2004).
- [34] K. Feitosa and D. J. Durian, *Eur. Phys. J. E* **26**, 309 (2008).
- [35] F. Bolton and D. Weaire, *Philos. Mag. B* **63**, 795 (1991).
- [36] D. Weaire, *Philos. Mag. Lett.* **79**, 491 (1999).
- [37] P. I. C. Teixeira and M. A. Fortes, *Philos. Mag.* **85**, 1303 (2005).
- [38] M. Mancini and C. Oguey, *Eur. Phys. J. E* **22**, 181 (2007).
- [39] F. Bolton and D. Weaire, *Philos. Mag. B* **65**, 473 (1992).
- [40] I. Fortuna, G. L. Thomas, R. M. C. de Almeida, and F. Graner, *Phys. Rev. Lett.* **108**, 248301 (2012).
- [41] H. Flyvbjerg, *Phys. Rev. E* **47**, 4037 (1993).
- [42] S. N. Chiu, *Materials Characterization* **34**, 149 (1995).
- [43] F. T. Lewis, *Anat. Rec.* **38**, 341 (1928).
- [44] F. T. Lewis, *Anat. Rec.* **47**, 59 (1930).
- [45] N. Rivier and A. Lissowski, *J. Phys. A: Math. Gen.* **15**, 143 (1982).
- [46] N. Rivier, *Phil. Mag. B* **52**, 795 (1985).
- [47] K. Y. Szeto and W. Y. Tam, *Physica A* **221**, 256 (1995).
- [48] J. Saraiva, P. Pina, L. Bandeira, and J. Antunes, *Philos. Mag. Lett.* **89**, 185 (2009).
- [49] M. Durand, J. Käfer, C. Quilliet, S. Cox, S. A. Talebi, and F. Graner, *Phys. Rev. Lett.* **107**, 168304 (2011).
- [50] S. Hilgenfeldt, A. M. Kraynik, S. A. Koehler, and H. A. Stone, *Phys. Rev. Lett.* **86**, 2685 (2001).
- [51] S. Hilgenfeldt, A. M. Kraynik, D. A. Reinelt, and J. Sullivan, *Europhys. Lett.* **67**, 484 (2004).
- [52] M. E. Glicksman, *Philos. Mag.* **85**, 3 (2005).
- [53] M. E. Glicksman, P. R. Rios, and D. J. Lewis, *Acta Materialia* **55**, 4167 (2007).